Geological Magazine

www.cambridge.org/geo

Palaeomagnetic dating of hydrothermal alteration in the Woodford Shale, Oklahoma, USA

Jennifer Roberts[1], Gerhard Heij[2] and R. Douglas Elmore[2,*]

[1]Chesapeake Energy, Oklahoma City, Oklahoma 73118, USA and [2]School of Geology and Geophysics, University of Oklahoma, Norman, Oklahoma 73019 USA

Original Article

Cite this article: Roberts J, Heij G, and Elmore RD (2019) Palaeomagnetic dating of hydrothermal alteration in the Woodford Shale, Oklahoma, USA. *Geological Magazine* **156**: 2043–2052. https://doi.org/10.1017/S0016756819000360

Received: 25 January 2019
Revised: 25 March 2019
Accepted: 28 March 2019
First published online: 6 June 2019

Keywords:
remagnetization; magnetite; open diagenetic system; timing fluid migration

Author for correspondence: R. Douglas Elmore, Email: delmore@ou.edu

Abstract

An oriented Woodford Shale core from the eastern Ardmore Basin was sampled to test if the shale was an open or closed system to hydrothermal fluids, and to determine the timing of alteration. Mineralized fractures are ubiquitous in the core, and the shale exhibits a complex paragenesis with multiple hydrothermal minerals, including biotite, magnesite, norsethite, gorceixite and potassium feldspar present in and around the fractures. These minerals suggest that the Woodford Shale was an open system during part of its diagenetic history. Vitrinite reflectance (R_o) measurements indicate values of ~1.81 % (~230 °C). Palaeomagnetic analysis reveals a characteristic remanent magnetization (ChRM) with south-southeasterly declinations and shallow inclinations that resides in magnetite. This ChRM is interpreted to be either a chemical remanent magnetization (CRM) or a thermochemical remanent magnetization (TCRM) that was acquired at 245 ± 10 Ma during Late Permian time based on the pole position (51.0° N, 115.6° E). Because the palaeomagnetic specimens show evidence of extensive hydrothermal alteration, the CRM/TCRM is interpreted to date the migration of hydrothermal fluids through the shale. The agreement in timing with other studies that report hydrothermal alteration in southern Oklahoma and the Ouachita Mountains in Late Permian time, suggest that there were post-collisional fluid-flow events which accessed reservoirs of warm fluids.

1. Introduction

Numerous studies have documented alteration by hydrothermal fluids in Palaeozoic rocks in the southern Midcontinent (e.g. Cathles & Smith, 1983; Bethke & Marshak, 1990; Elmore *et al.* 1993; Garven *et al.* 1993 and numerous others). Most of these studies focused on ore deposits and carbonates. Estimates of the timing based on radiometric and palaeomagnetic techniques generally cover a wide age range in the late Palaeozoic period (e.g. Leach *et al.* 2001). A number of mechanisms have been proposed for the origin of the hydrothermal deposits, with most studies suggesting a connection with collisional tectonics and uplift (e.g. Bethke & Marshak, 1990; Garven *et al.* 1993). Determining the timing of hydrothermal alteration can provide important constraints on the origin of the hydrothermal fluids.

The objective of this study is to test the timing and origin of hydrothermal alteration in the Woodford Shale, an important source rock and unconventional reservoir (Cardott, 2012; Kennedy *et al.* 2014), in an oriented core from the Ardmore Basin, southern Oklahoma (Core B; Fig. 1a). A recent study of the Woodford Shale (Upper Devonian – lower Mississippian) indicates that the unit contains hydrothermal minerals in two cores in the Anadarko Basin in Oklahoma (Roberts & Elmore, 2018). Alteration by hydrothermal fluids will be tested in the Ardmore Basin core based on petrographic observations, and the timing of alteration will be determined using palaeomagnetic analysis (e.g. Elmore *et al.* 2012). The results will be compared to the timing of other hydrothermal events in the Midcontinent (e.g. Shelton *et al.* 1986; Garven *et al.* 1993; Leach *et al.* 2001).

The results of the study also have implications for our understanding of shales, which can be diagenetically complex and heterogeneous (e.g. Milliken *et al.* 2012; Kennedy *et al.* 2014). While progress has been made understanding shale diagenesis, several fundamental issues still need to be investigated, including how shales evolve and whether they behave as open or closed systems (e.g. Land *et al.* 1997; Bjorlykke & Jahren, 2012). One reason for the mineralogical heterogeneity in shales could be alteration by external fluids.

2. Geologic setting

Between the late Cambrian and Mississippian period, up to ~3 km of mostly carbonate and shale sequences were deposited in the southern Oklahoma trough, including the Woodford Shale (Perry, 1989). During the Ouachita orogeny (late Mississippian to late Pennsylvanian), the trough was divided into sub-basins including the Ardmore Basin (Granath, 1989). The Ardmore Basin is within the foreland of the Ouachita fold belt, and is bounded by faults

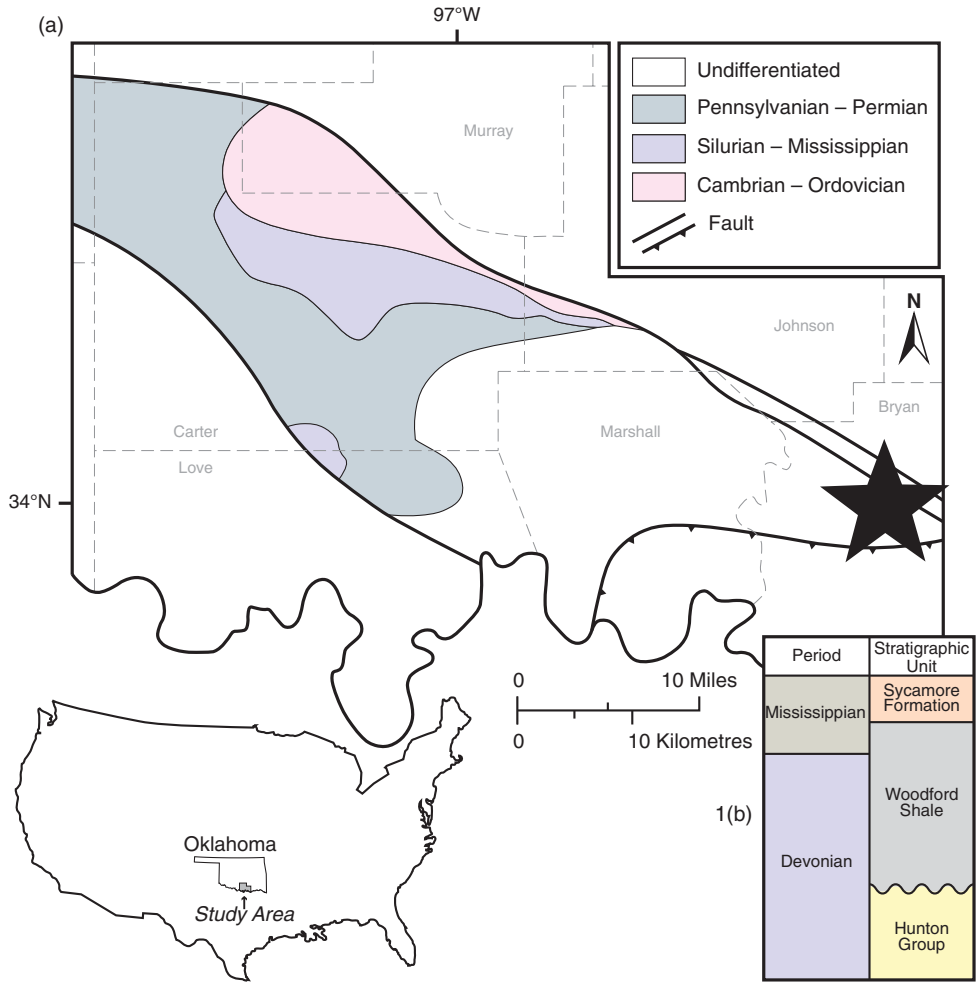

Fig. 1. (a) Simplified geologic map of the Ardmore Basin showing major rock units and faults in the basin (after Northcutt & Campbell, 1998). Map of the United States shows location of Oklahoma and the study area. The star indicates the location of Core B. 'Undifferentiated' refers to Cretaceous and Quaternary rocks. (b) Simplified stratigraphic section from the study area. Adapted by permission from Springer Nature: Springer: Geologic Provinces of Oklahoma, RA Northcutt & JA Campbell, © 1998.

(Fig. 1a) which were part of a left-lateral fault system that evolved into a transpressive system in Pennsylvanian time (Granath, 1989). During Pennsylvanian deformation, the rocks in the Ardmore Basin were folded, faulted and uplifted, resulting in the structural complexity observed today (Granath, 1989). As a result of the deformation, unconformities and syntectonic conglomerates (e.g. Collings Ranch) are present in the Pennsylvanian section (Granath, 1989).

The Woodford Shale is an organic-rich, siliceous black shale with interbedded light-coloured shale, siltstone, dolostone and chert (Miceli Romero & Philp, 2012) deposited in restricted marine, hypersaline and potentially lacustrine environments (Infante-Paez *et al.* 2017). The high organic content present in the Woodford Shale is due to the primarily anoxic conditions it was deposited under and slow sedimentation rates, with its variability caused by sea-level fluctuations and topographic relief influencing ocean circulation and oxygenation during deposition (Kirkland *et al.* 1992). The Woodford Shale unconformably overlies the Hunton Group (Chimneyhill Subgroup, Henryhouse Shale, Haragan Shale and Bois d'Arc Limestone) and is conformably overlain by the Sycamore Limestone in the Ardmore Basin (Fig. 1b). The unconformity surface contains considerable topographic relief due to incised valleys and karst features that formed during subaerial exposure resulting from drops in eustatic sea-level (Infante-Paez *et al.* 2017).

Several studies report on the diagenesis of the Woodford Shale in the Anadarko Basin (e.g. Chalmers *et al.* 2012; Cardott, 2013; Laughrey *et al.* 2017; Roberts & Elmore, 2018). Roberts & Elmore (2018) reported that the Woodford Shale contains hydrothermal minerals such as magnesite ($MgCO_3$), norsethite ($BaMg(CO_3)_2$), gorceixite ($BaAl_3(PO_4)(PO_3OH)(OH)_6$) and potassium feldspar in two cores from the southern part of the Anadarko Basin to the west and north of the Ardmore Basin. The absolute timing for precipitation of these minerals is unknown, although they are interpreted to have precipitated during middle–late diagenesis, mostly in and around mineralized fractures.

3. Methodology

Core B contains a total of 55 m (179 ft) of Woodford Shale, with depths ranging from 1011–1066 m (3317–3496 ft) and was oriented using the scribe method (Nelson *et al.* 1987). The core is vertical and the bedding is horizontal. A fault occurs ~600 m (~2000 ft) above the Woodford Shale and there are some faults within the Woodford Shale. Most specimens (87 %) contain mineralized fractures (Fig. 2a) or are within 6 cm of an obvious

https://doi.org/10.1017/S0016756819000360 Published online by Cambridge University Press

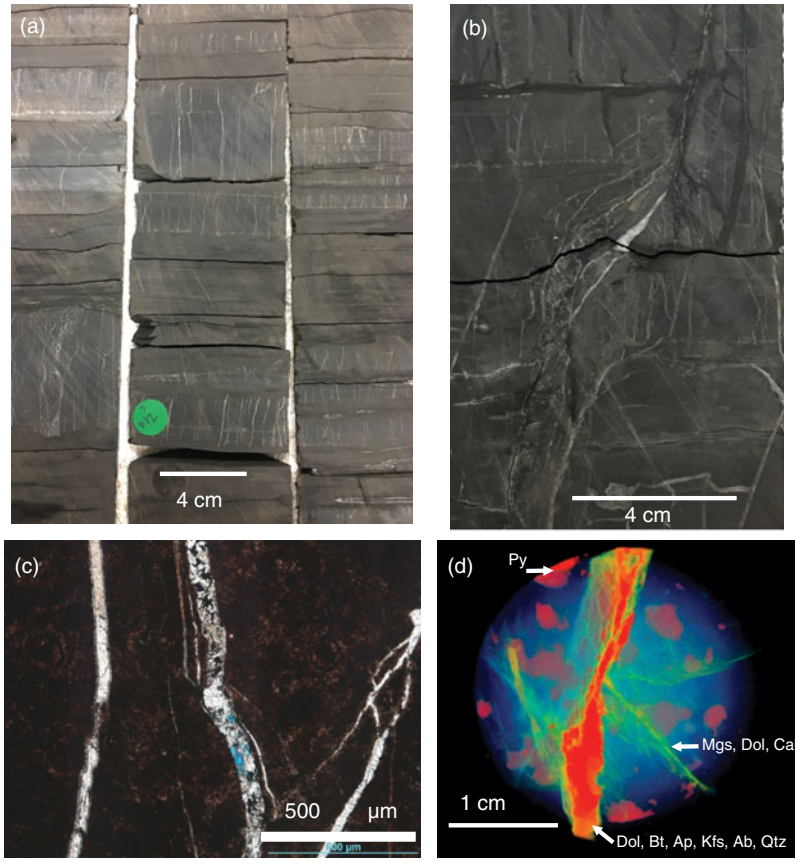

Fig. 2. (a, b) Photographs of representative core sections showing the, mostly vertical, mineralized fractures. Most fractures occur in siliceous beds. (c) Thin-section photomicrograph of siliceous shale with mineralized fractures filled with calcite and dolomite (plane-polarized light, PPL). (d) XRCT scan of sample illustrating the fractures in the sample. The less dense material (blue) has been largely removed, which shows the more dense mineralized fractures (red and green, red highest density) in three dimensions. Minerals in the fractures were identified based on SEM-EDS and thin-section analysis (see Fig. 3) of the core. (Dol – dolomite; Bt – biotite; Ap – apatite; Kfs – potassium feldspar; Ab – albite; Mgs – magnesite; Qtz – quartz; Py – pyrite; Cal – calcite)

fracture. The 'butt' sections of the vertical core were drilled normal to the bedding using a fixed, variable-speed, water-cooled drill press with a non-magnetic core bit, and oriented relative to the scribe line and the stratigraphic up direction. Core plugs were cut into standard palaeomagnetic specimens (2.54 diameter x 2.2 cm) and chips were used for thin-sections.

Thirty-five polished thin-sections were examined using a petrographic microscope in both reflected and transmitted light and using a scanning electron microscope (SEM) with an electron dispersive spectrometer (EDS). The focus of the petrographic study was on mineralized fractures. Minerals were identified based on their habits and elemental composition, and their relative timing was determined by textural relationships. X-ray computed tomography scans (XRCT) were conducted on 2.5 cm plugs from the core to further characterize fracture networks and upscale features seen on the petrographic scale. XRCT data from Core B was obtained from the University of Minnesota using a X5000 high-resolution micro-CT system with a twin head 225 kV FeinFocus FXE-225.99 X-ray tube and Dexela 2923 area detector.

A Vickers M17 Research Microscope system adapted for reflected white light on slides immersed in oil at a magnification of 500× was used to obtain vitrinite and bitumen reflectance data from in and around mineralized fractures. The bitumen reflectance data was used to calculate vitrinite reflectance equivalent (VRE) values for thermal maturity (Landis & Castaño, 1994; Schoenherr *et al.* 2007). Fluid inclusions in calcite and barite from mineralized fractures were examined but were too small to determine homogenization temperatures or compositions.

Thirty-four specimens collected from the core were subjected to stepwise, thermal demagnetization and were measured in a 2G-Enterprises cryogenic magnetometer with a direct current superconducting quantum interference device in a magnetically shielded room. In addition, three specimens were subjected to alternating field (AF) demagnetization up to 120 mT in 10 mT increments. Demagnetization data was plotted on orthogonal diagrams, from which magnetic components were found using principal component analysis (Kirschvink, 1980). Magnetic components with the maximum angular deviation (MAD) less than 18° were selected to calculate mean statistics (Fisher, 1953).

Rock magnetic experiments were also performed to identify the magnetic mineralogy. Hysteresis loops were acquired on representative samples on a Princeton Measurements vibrating sample magnetometer (VSM) 3900-04 at Southern Illinois University Carbondale. An applied field of 0.5 Tesla (T) was applied to saturate the samples with a field step of 2.5 mT and averaging time of 0.5 s, which allowed for maximum signal to noise ratio. The paramagnetic slope correction and a moderate moving window smoothing was applied to raw hysteresis loops (e.g. Jackson & Solheid, 2010; Paterson *et al.* 2018). Hysteresis parameters (remanent magnetization, Mrs; saturation magnetization, Ms; and coercivity, Bc) were computed from processed loops. Back-field

https://doi.org/10.1017/S0016756819000360 Published online by Cambridge University Press

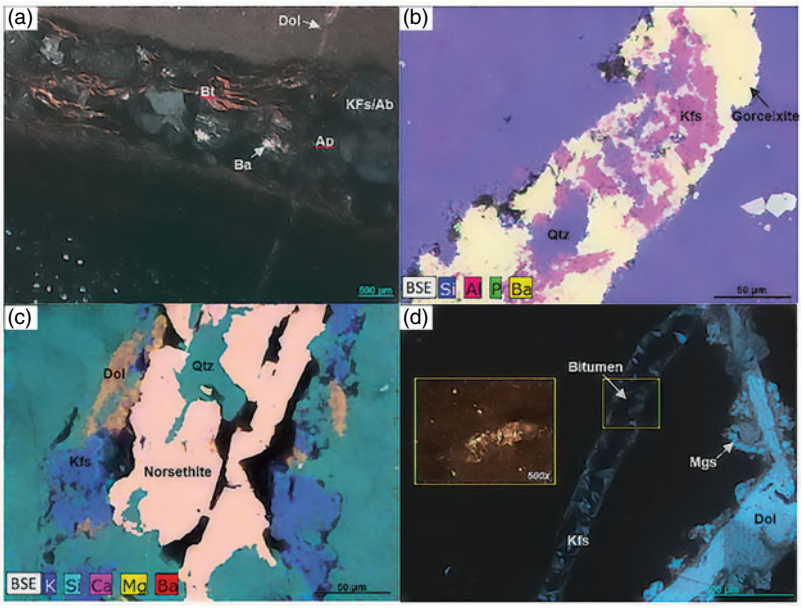

Fig. 3. Hydrothermal and diagenetic features/minerals. (a) Photomicrograph displaying a horizontal fracture filled with biotite, potassium feldspar as well as apatite and barite. The horizontal fracture is cut by a vertical dolomite-filled fracture (cross-polarized light, CPO). (b) Backscattered electron (BSE) image with elements based on an energy dispersive spectroscopy (EDS) overlay displaying a fracture filled with gorceixite (yellow-green-pink), potassium feldspar (pink-blue) and quartz (blue). (c) BSE image with an EDS overlay and the interpreted phases. The fracture contains dolomite (orange), potassium feldspar (blue), norsethite (red-yellow) and quartz (cyan). (d) Fracture containing dolomite and magnesite, and another containing potassium feldspar and pyrobitumen. Note that magnesite extends into the matrix. The pyrobitumen is displayed in a reflected-light image (yellow box) and was used to obtain bitumen reflectance values (CPO). (Dol – dolomite; Bt – biotite; Ba – barite; Ap – apatite; Kfs – potassium feldspar; Ab – albite; Mgs – magnesite; Qtz – quartz; Py – pyrite)

measurements were measured to obtain remanent coercivity (Bcr). Isothermal remanent magnetization (IRM) acquisition curves were acquired in order to determine the contribution of magnetic carrier minerals. The IRM curves were analysed using the Max Unmix program (Maxbauer *et al.* 2016) to determine the coercivity spectrum of the samples. A Monte-Carlo style resampling routine was used for error analysis. The 95 % confidence intervals were used to display uncertainty in each modelled component distributions.

4. Results and interpretations

The stratigraphy of the Woodford Shale in the core is dominated by cherty and siliceous facies (Fig. 2a), with the least common facies being argillaceous and dolomitic. The lower section of the Woodford Shale is characterized by siliceous and argillaceous facies with sparse grey silty laminae which decrease up section where cherty and siliceous facies that are either massive or contain faint dark grey laminae dominate. Mineralized fractures are ubiquitous (Fig. 2a–d), particularly in the siliceous and cherty facies (Fig. 2b), and some brecciation is also present. Most mineralized fractures are vertical to subvertical and occur in siliceous beds (Fig. 2a–c). The XRCT analysis illustrates large millimetre-scale mineralized fractures with higher density mineral assemblages and relatively lower density mineral assemblages in the subordinate (< 1 mm) fractures (Fig. 2d).

The Woodford Shale displays a complex paragenesis (Fig. 3). Events within the matrix and allochems occurred primarily during early diagenesis whereas events associated with fracturing dominate late diagenesis. The most common allochems present are Radiolaria and *Tasmanites*. Events interpreted as early based on petrographic relationships include precipitation of pyrite (Fig. 2d), formation of phosphate nodules with barite and silica filling pores within the nodules, and quartz overgrowths.

Mineralized fractures contain multiple minerals, including potassium feldspar, albite, quartz, barite, norsethite, pyrite, gorceixite, apatite, biotite and magnesite (Fig. 3a–d), and are interpreted as forming during middle–late diagenesis. Biotite occurs in a horizontal fracture-fill in association with potassium feldspar (Fig. 3a), interpreted as adularia based on its blocky habit (Deer *et al.* 1963). The minerals such as magnesite commonly extend from the fractures into the matrix (Fig. 3d). Fractures filled with megaquartz, calcite and dolomite are common. Six vitrinite reflectance values were obtained having an average R_o value of 1.81 % (standard deviation = 0.07; n = 5), equating to a maximum heating temperature of ~230 °C (Barker & Pawlewicz, 1986). Two VRE values (1.47 and 1.57 %) for bitumen (Fig. 3d) are consistent with a maximum heating temperature of ~210 °C (Barker & Pawlewicz, 1986).

Thermal demagnetization reveals two magnetic components present in Core B. A poorly defined viscous remanent magnetization with a north-northwesterly declination and a moderate-steep down inclination is unblocked at low temperatures (natural remanent magnetization to ~150 °C; Fig. 4a). At higher temperatures (200 to 400–425 °C), a characteristic remanent magnetization (ChRM) is unblocked with south-southeasterly declinations and shallow inclinations (Fig. 4a–d). Above 400–425 °C the magnetic intensity increases in many specimens, likely due to the creation of magnetite by oxidation of pyrite. The mean ChRM direction from thermal demagnetization is declination (D) 160.5° and inclination (I) 1.1° (Table 1).

A preliminary set of specimens was subjected to AF demagnetization, which isolated ChRM from 20–120 mT with southeasterly declinations and moderate down inclinations (D = 154.0°, I = 26.4 °; Table 1). The ChRM isolated by AF demagnetization displays a steeper inclination than the ChRM revealed by thermal demagnetization. This discrepancy probably indicates a partial

https://doi.org/10.1017/S0016756819000360 Published online by Cambridge University Press

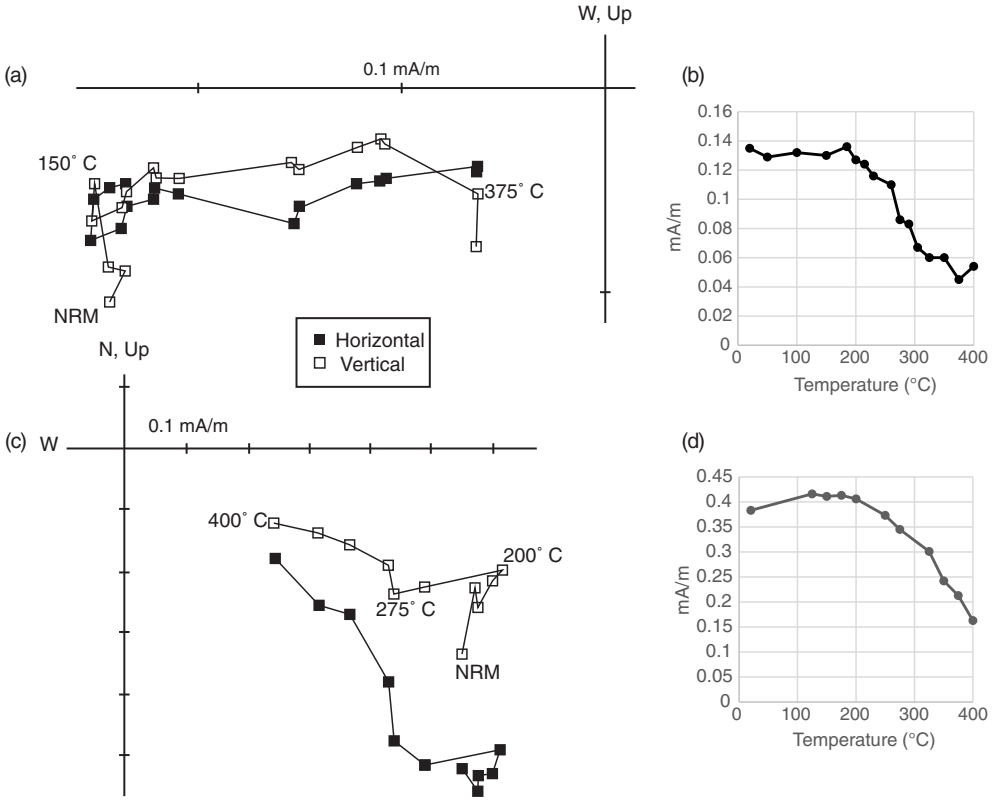

Fig. 4. Thermal demagnetization data. (a) Orthogonal plot (*in situ* directions) of thermal demagnetization for specimen S23 (closed squares – horizontal component; open squares – vertical component). (b) Thermal decay of natural remanent magnetization (NRM) for specimen in (a). (c) Orthogonal plot of thermal demagnetization for specimen S29 (*in situ* directions). (d) Thermal decay of NRM for specimen in (c).

contamination of the ChRM by a modern component during AF treatment (e.g. McCabe *et al.* 1984); therefore, the specimen directions obtained from AF demagnetization were excluded from determining the mean direction.

The ChRM is revealed in 24 of the 34 specimens during thermal demagnetization (Fig. 5; Table 1) which span the core and are present in those intervals that are highly altered by mineralized fractures. Of the remaining ten specimens, five contain what is interpreted as the ChRM, but their MAD angles were unacceptable (> 18°) and five exhibit weak, unstable magnetizations. A virtual geomagnetic pole (VGP) for the mean (*in situ*) isolated from thermal demagnetization (51.0° N, 115.6° E; Table 1) plots on the apparent polar wander path (APWP) for North America at 245 ± 10 Ma, consistent with a Late Permian age (Fig. 6).

The samples have very weak magnetizations. A representative hysteresis loop is slightly wasp-waisted (Fig. 7a–c) and is consistent with a mixed magnetic assemblage or a mixture of grain sizes (e.g. Tauxe *et al.* 1996). The Ms value is 3.3e−08 Am^2, the Mrs value is 5.91e−09 Am^2, the Bc is 13.1 mT and the Bcr is 22.9 mT. The Mr/Mrs and Bc/Bcr ratios are consistent with pseudo single domain (PSD) magnetite. A separation of the loop at high fields is interpreted to indicate thermal drift and pole saturation artefacts.

Unmixing of IRM acquisition data can be modelled using one or two components (Fig. 8). Most specimens were modelled with one component with the mean log coercivity (Bh) ranging from 1.75 to 1.84 (Fig. 8a). These results are consistent with ranges for magnetite reported by Egli (2003). For the two-component modelling, the observed contribution (OC) of component 1 is 0.65 with a Bh of 1.72 (Fig. 8b), consistent with magnetite. The OC for component 2 is 0.35 with a mean Bh of 2.2 (Fig. 8b). Component 2 has a relatively broad coercivity range and probably resides in haematite, although it is not interpreted to carry a stable remanence based on the demagnetization characteristics.

5. Discussion

Based on unblocking temperatures and the rock magnetic data, the ChRM is interpreted to reside in magnetite. The relatively high temperatures interpreted from the vitrinite and bitumen reflectance data could have exerted an influence on the acquisition of the ChRM. A thermoviscous remagnetization is possible based on the unblocking temperatures (425 °C) and heating temperatures (210–230 °C) for multi-domain magnetite (e.g. Dunlop & Ozdemir, 1997, p. 281). The timing of the Late Permian ChRM, however, is not consistent with timing of deformation and uplift, which occurred in late Pennsylvanian time (Granath, 1989). There is no evidence for significant faulting younger than late Pennsylvanian, and the rocks were at relatively shallow depths (< 1066 m) in Late Permian time. Burial heating and uplift would presumably have caused a thermoviscous remagnetization in late Pennsylvanian not Late Permian times. This suggests that a thermoviscous mechanism caused by burial heating is not likely.

The palaeomagnetic evidence indicates there was one major episode of chemical remagnetization. The specimens with the ChRM contain hydrothermal alteration and the magnetite is interpreted to have formed from the hydrothermal fluids. Although magnetite was not observed based on the petrographic studies, it is a common mineral that is found in association with other hydrothermal minerals (Nadoll *et al.* 2014). The ChRM is interpreted as

https://doi.org/10.1017/S0016756819000360 Published online by Cambridge University Press

Table 1. Summary of palaeomagnetic data

Component	Dec	Inc	k	α95	N/No	Pole Lat	Pole Long	dp	dm
ChRM	160.5°	1.1°	9.1	10.4°	24/34	51.0° N	115.6°E	5.2°	10.4°
AF	154.0°	26.4°	29.8	23°	3/3	-	-	-	-

Note: N/No – Number of specimens accepted for statistical purposes versus number of specimens demagnetized; Dec – declination; Inc – inclination; α95 – 95 % cone of confidence; k – Fisher's (1953) best estimate of the precision parameter; Lat – latitude; Long – longitude; dp, dm – semiaxes of 95 % cone of confidence of pole. AF under component refers to specimens subjected to alternating field demagnetization in a pilot study.

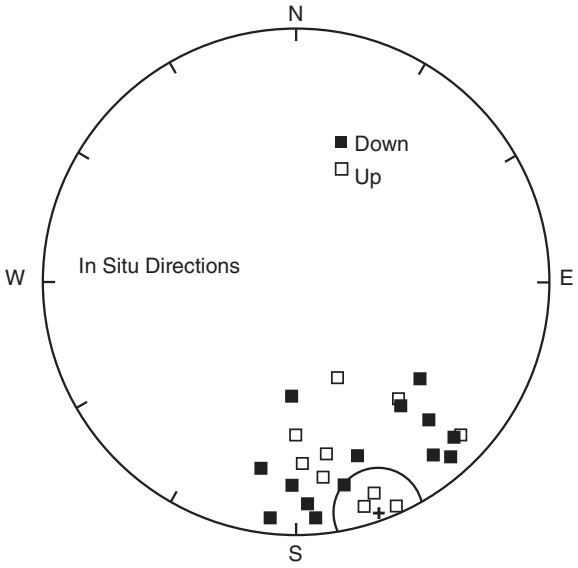

Fig. 5. Equal-area projection of the *in situ* ChRM specimen directions. The plus symbol is the mean direction and its surrounding circle is the α_{95} confidence limit. Closed squares – down inclinations; open squares – up inclinations.

either a chemical remanent magnetization (CRM) that formed from the chemical growth of magnetite or thermochemical remanent magnetization (TCRM) that formed from a combination of magnetite growth and cooling from the hot fluids (Dunlop & Ozdemir, 1997, p. 409).

The difference in timing between the likely time of maximum burial (late Pennsylvanian) and the CRM age (Late Permian) suggests that a burial remagnetization mechanism (e.g. Aubourg *et al.* 2012; Elmore *et al.* 2012) is not likely. The Woodford Shale in the core is at 1011–1066 m (3100–3500 ft), which would not result in burial temperatures of 210–230°. If maximum burial as well as significant faulting and uplift occurred in Late Permian time, however, then a burial diagenetic mechanism and/or thermoviscous remagnetization is a possibility. There is no evidence for Late Permian uplift, and we conclude that a burial diagenetic mechanism and/or thermoviscous remagnetization are not supported by the geological history and the age of the magnetization. It is possible, however, that the hot fluids may have triggered burial diagenetic processes (e.g. Aubourg *et al.* 2012) such as maturation of organic matter or clay diagenesis in the matrix in Late Permian time, but if this is the case, the CRM or TCRM would still date the migration of hydrothermal fluids.

Numerous minerals in the Woodford Shale suggest alteration by hydrothermal fluids, including magnesite (Shand, 2006), norsethite (e.g. Steyn & Watson, 1967; Bötcher, 2000), apatite (e.g. Bouzari *et al.* 2016), gorceixite (Migaszewski *et al.* 2007), biotite (Wang *et al.* 2014) and potassium feldspar (Shelton *et al.* 1986). The abundance of quartz-filled fractures in the core suggests the necessary pressure–temperature conditions were reached to cause the dissolution and precipitation of silica within a hydrothermal system (e.g. Okamoto *et al.* 2010). The relatively high R_o and VRE values suggest temperatures of 210–230 °C, which is consistent with at least localized alteration by hydrothermal fluids.

Some of the minerals, such as norsethite (Mrose *et al.* 1961) and albite (Kastner, 1971), have been found as authigenic minerals in rocks that are not hydrothermally altered. The abundance of likely hydrothermal minerals and the temperature data (210–230 °C), however, are consistent with the hydrothermal fluid interpretation.

The source for some of the elements in the minerals could have been the basement or from the Woodford Shale. For example, the K in the feldspar and the Mg could have been derived from minerals in the basement. Alternatively, the Mg might have come from dewatering of the shale or the smectite to illite conversion. The Ba and P, however, could also have been derived from the basement, although they could also come from shales. Barite can form relatively early (Zhou *et al.* 2015), produced by bacterial activity in the sediment (e.g. González-Muñoz *et al.* 2003), and then can be remobilized in strongly reducing environments (Hanor, 2000) to form in mineralized fractures. Phosphate can also form during early diagenesis (e.g. Li & Schieber, 2015). Quartz could have been derived from hydrothermal fluids (e.g. Shelton *et al.* 1986), biogenic silica (e.g. Milliken & Olson, 2017), shale dewatering or from silica released during the conversion of smectite to illite (e.g. Land *et al.* 1997).

The open versus closed issue has been controversial (e.g. Land *et al.* 1997; Bjorlykke & Jahren, 2012) and remains an important fundamental issue in shale diagenesis, partly because it relates to reservoir quality. Shales can be open during early diagenesis and can evolve to a closed system during burial (Bjorlykke & Jahren, 2012), although migration of hydrothermal fluids into a shale during and after deformation can establish an open system. The results from this study imply that warm hydrothermal fluids entered the shale during late diagenesis. They probably carried some elements that formed the hydrothermal minerals, although they may have leached some elements from the shale.

The Late Permian age for the hydrothermal event in the Woodford Shale is younger than many other fluid-related and burial diagenetic events in the Arbuckle Mountains and north-central Oklahoma, which range in age from late Pennsylvanian to Early Permian (Elmore, 2001; Elmore *et al.* 2018). The timing of alteration in the Woodford Shale is also younger than some Mississippi Valley-type (MVT) mineralization in the Midcontinent, although it is generally consistent with the timing of mineralization in northern Arkansas (Leach *et al.* 2001). The timing of alteration in the Woodford Shale is generally consistent with the second or third stage of a hypothesized three-stage set of hydrothermal events that affected lower and middle Palaeozoic carbonate units north of the study area in southeastern Kansas, northeastern Oklahoma and southwest Missouri (Goldstein & King, 2014). Stage one altered

https://doi.org/10.1017/S0016756819000360 Published online by Cambridge University Press

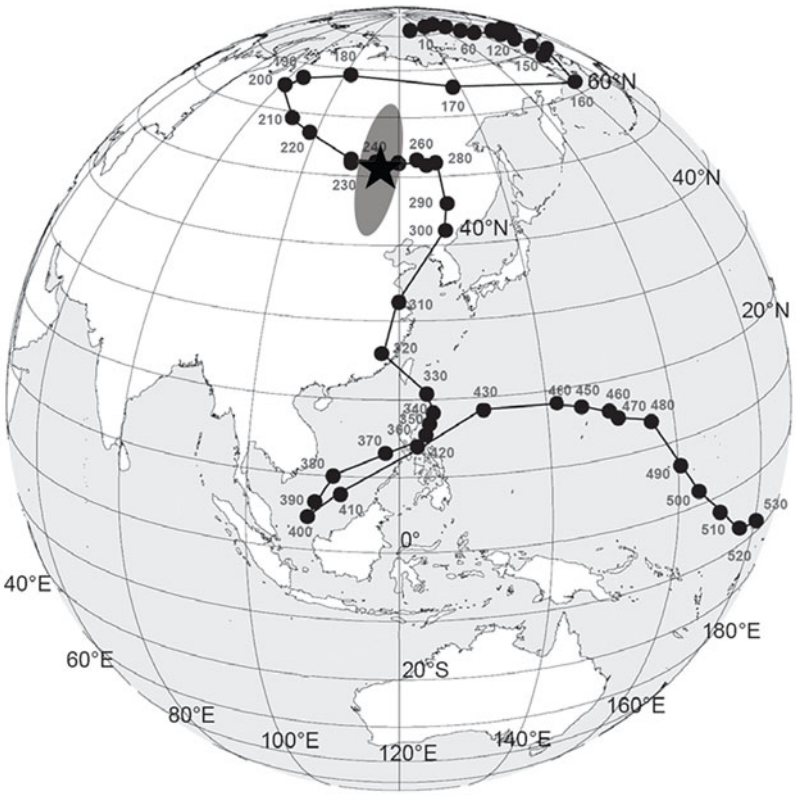

Fig. 6. North American APWP (data from Torsvik *et al*. 2012) with the pole for the ChRM (star) and the 95 % confidence ellipse. The age of the Woodford Shale is Late Devonian – early Mississippian (~375–360 Ma). The pole for the ChRM intersects the path at 245 ± 10 Ma in the Late Permian. The error is based on the extent of the 95 % ellipse as plotted on the APWP.

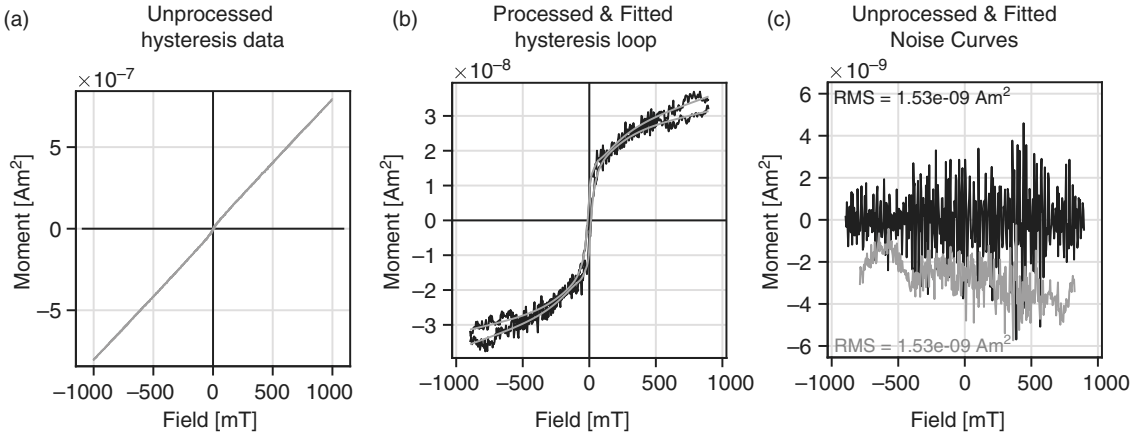

Fig. 7. (a) Representative unprocessed hysteresis loop, (b) processed and fitted hysteresis loop with the paramagnetic slope removed, and (c) the unprocessed (grey) and fitted (black) noise curves. Data processed following Paterson *et al*. (2018).

Ordovician and Mississippian strata, and was inferred to be late Pennsylvanian – Early Permian in age and related to the Ouachita orogeny and gravity-driven flow. Stage two was characterized by precipitation of baroque dolomite in the carbonate units, and was inferred to be Permian in age, of regional extent and affected by Ouachita tectonics. Stage three resulted in calcite precipitation, was more localized and was interpreted to be after the main phase of Ouachita tectonic activity. We note, however, that the study area for the Goldstein and King study was north of the Ardmore Basin, and the nature of the hydrothermal minerals that precipitated was different, suggesting it may have been a different hydrothermal system. Garven *et al*. (1993), based on modelling studies, proposed that late Pennsylvanian uplift of the Ouachita Mountains caused gravity-driven flow of fluids to the north. They also pointed out that the flow systems dissipated in Late Permian – Early Triassic times because of erosion of the uplifts.

Several studies conducted in the region also indicate alteration by hydrothermal fluids in Late Permian time. For example, Shelton *et al*. (1986) found Ba-rich adularia in the Upper Ordovician Womble Shale in the Ouachita Mountains with a K–Ar date of

https://doi.org/10.1017/S0016756819000360 Published online by Cambridge University Press

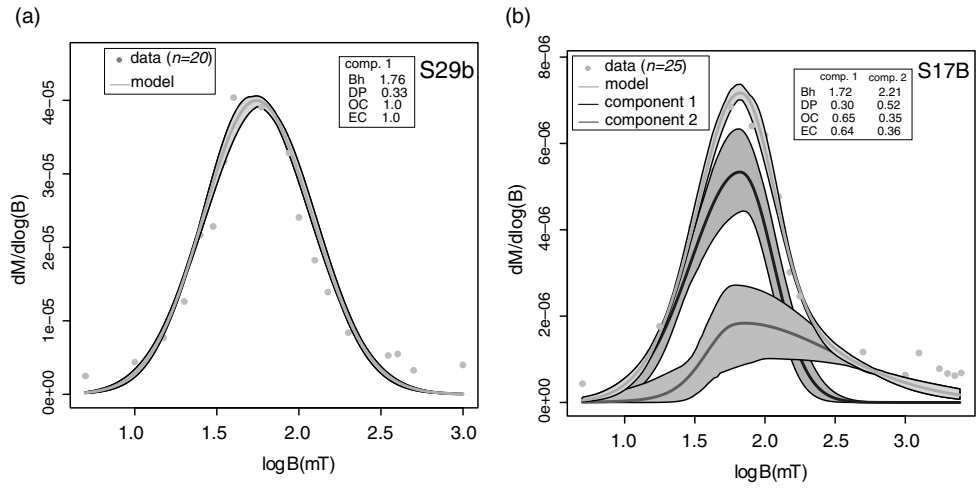

Fig. 8. Representative model fits of coercivity spectrums. Shaded areas represent 95 % error envelopes of the model and the components. Most samples were modelled with one component (a), which is interpreted to be magnetite. A sample modelled with two components is shown in (b). Component 1 likely corresponds to magnetite whereas component 2 represents a higher coercivity mineral such as haematite. Component 2 is not interpreted to carry a remanence based on the demagnetization characteristics. OC – mean observed contribution; EC – estimated contribution; DP – Dispersion parameter; Bh – mean log coercivity.

262 ± 10 Ma that is associated with post-folding quartz veinlets. Fluid inclusion data yielded a maximum formation temperature of 300 °C. The mechanism proposed for this event was post-folding faulting in the Ouachita Mountains that accessed a reservoir of hot hydrothermal fluids. Elmore *et al.* (1993) found alteration by warm fluids with elevated $^{87}Sr/^{86}Sr$ values in and around fault-related veins mineralized with MVT minerals in the Viola Limestone in the Arbuckle Mountains. Haematite alteration around veins was dated using palaeomagnetic data to the Late Permian.

The Late Permian timing for alteration in the Woodford Shale may have implications for the mechanism of hydrothermal fluid flow since one of the most popular mechanisms, gravity-driven flow from highlands (e.g. Garven *et al.* 1993), is not likely because of low relief in southern Oklahoma in Late Permian time (Johnson, 1989). Another mechanism, such as fluid flow along Pennsylvanian faults, perhaps reactivated, in Late Permian time, is a possibility. The fact that Core B cuts through a fault ~600 m (~2000 ft) above the Woodford Shale and that faulting is common in the study area (Marsh & Holland, 2016) is consistent with this interpretation. The coincidence of three events at about the same age in southern Oklahoma (this study; Shelton *et al.* 1986; Elmore *et al.* 1993) are consistent with a similar origin, such as migration of hydrothermal fluids along faults.

6. Conclusions

Numerous minerals found largely in mineralized fractures in a core from the Ardmore Basin (southern Oklahoma), such as norsethite, potassium feldspar, albite, gorceixite, biotite, magnesite and quartz, and in the matrix, suggest that the Woodford Shale has been altered by hydrothermal fluids. The R_o and VRE values yield a maximum temperature of 210–230 °C. Palaeomagnetic results from the oriented core indicate a CRM or TCRM residing in magnetite that formed in Late Permian time. The palaeomagnetic data, significant quantities of hydrothermal minerals and the high thermal maturities suggest that the Woodford Shale was altered by externally derived fluids in Late Permian time. This suggests that the Woodford Shale was an open system in the Late Permian period. The agreement in timing with other studies which report hydrothermal alteration in southern Oklahoma and eastern Arkansas (e.g. Shelton *et al.* 1986; Elmore *et al.* 1993) suggest there may have been widespread post-collisional fluid-flow events in late Palaeozoic time in the Midcontinent.

Author ORCIDs. Richard Elmore 0000-0003-0062-6276

Acknowledgements. The authors thank Chesapeake Energy for supplying the core. We thank Brian Cardott for collecting the vitrinite and bitumen reflectance data and Eric Ferré for providing the hysteresis data. The authors thank two anonymous reviewers for helpful suggestions. This research did not receive any specific grant from funding agencies in the public, commercial or not-for-profit sectors.

Declaration of Interest. Jennifer Roberts works for Chesapeake Energy in Oklahoma City. The manuscript was submitted to Chesapeake for approval, which was granted.

References

Aubourg C, Pozzi J and Kars M (2012) Burial, claystones remagnetization and some chemical consequences for magnetostratigraphy. In *Remagnetization and Chemical Alteration of Sedimentary Rock* (eds RD Elmore, AR Muxworthy, MM Aldana and M Mena), pp. 181–8. Geological Society London, Special Publication no. 371.

Barker CE and Pawlewicz MJ (1986) The correlation of vitrinite reflectance with maximum temperature in humic organic matter. *Paleogeothermics: Springer-Verlag, Lecture Notes in Earth Sciences* **5**, 79–93.

Bethke CM and Marshak S (1990) Brine migrations across North America – the plate tectonics of groundwater. *Annual Review of Earth and Planetary Sciences* **18**, 287–315.

Bjorlykke K and Jahren J (2012) Open or closed geochemical systems during diagenesis in sedimentary basins: constraints on mass transfer during diagenesis and the prediction of porosity in sandstone and carbonate reservoirs. *American Association of Petroleum Geologists Bulletin*, **96**, 2193–214.

Bötcher M (2000) Stable isotope fractionation during experimental formation of norsethite (BaMg[CO3]2): a mineral analogue of dolomite. *Aquatic Geochemistry* **6**, 201–12.

Bouzari FB, Hart CJR, Bissig T and Barker S (2016) Hydrothermal alteration revealed by apatite luminescence and chemistry: a potential indicator mineral for exploring covered porphyry copper deposits. *Economic Geology* **111**, 1397–410.

Cardott BJ (2012) Thermal maturity of Woodford Shale gas and oil plays, Oklahoma, USA. *International Journal of Coal Geology* **103**, 109–19.

https://doi.org/10.1017/S0016756819000360 Published online by Cambridge University Press

Cardott BJ (2013) Woodford Shale: from hydrocarbon source rock to reservoir. AAPG Search and Discovery Article #50817.

Cathles LM and Smith AT (1983) Thermal constraints on the formation of the Mississippi Valley-type lead-zinc deposits and their implications for episodic basin dewatering and deposit genesis. *Economic Geology* **78**, 983–1002.

Chalmers GR, Bustin RM and Power M (2012) Characterization of gas shale pore systems by porosimetry, pycnometry, surface area, and field emission scanning electron microscopy/transmission electron microscopy image analyses: examples from the Barnett, Woodford, Haynesville, Marcellus, and Doig units. *American Association Petroleum Geologists Bulletin* **96**, 1099–119.

Deer WA, Howie RA and Zussman J. (1963) *Rock-Forming Minerals: Framework Silicates*. London: Longmans, Green and Co., 528 pp.

Dunlop DJ and Ozdemir O (1997) *Rock Magnetism: Fundamentals and Frontiers*. New York: Cambridge University Press 573 pp.

Egli R (2003) Analysis of the field dependence of remanent magnetization curves. *Journal of Geophysical Research* **108**, B2, 2081. doi: 10.1029/2002JB002023.

Elmore RD (2001) A Review of paleomagnetic data on the timing and origin of multiple fluid-flow events in the Arbuckle Mountains, southern Oklahoma. *Petroleum Geoscience* **7**, 223–9.

Elmore RD, Haynes J, Farzaneh S and Anzaldua S (2018) Integrated paleomagnetic and diagenetic study of the Mississippian Limestone, North Central Oklahoma. In *Mississippian Reservoirs of the Midcontinent* (eds GM Grammer, JM Gregg, JO Puckette, P Jaiswal, SJ Mazzullo, MJ Pranter and RH Goldstein). American Association of Petroleum Geologists Memoir 116, doi: 10.1306/13632156M11667.

Elmore RD, London D, Bagley D, and Fruit D (1993) Remagnetization by basinal fluids: testing the hypothesis in the Viola Limestone, southern Oklahoma. *Journal of Geophysical Research* **98**, 6237–54.

Elmore RD, Muxworthy AR and Aldana M (2012) Remagnetization and chemical alteration of sedimentary rocks. In *Remagnetization and Chemical Alteration of Sedimentary Rock* (eds RD Elmore, AR Muxworthy, MM Aldana and M Mena), pp. 1–21. Geological Society of London, Special Publication no. 371.

Fisher RA (1953) Dispersion on a sphere. *Geophysical Journal of the Royal Astronomical Society* **217**, 295–305.

Garven G, Ge S, Person MA and Sverjensku DA (1993) Genesis of stratabound ore deposits in the Midcontinent basins of North America; 1, the role of regional groundwater flow. *The American Journal of Science* **293**, 497–568.

Goldstein RH and King BD (2014) Impact of hydrothermal fluid flow on Mississippian reservoir properties, southern Midcontinent. *Unconventional Resources Technology Conference, Denver, Colorado, USA, 25–27 August, URTeC-1934915-MS*, 8 pp. doi: 10.15530/urtec-2014-1934915.

González-Muñoz MT, Fernandez-Luque B, Martinez-Ruiz F, Ben Chekroun K, Arias JM, Rodriguez-Gallego M and Paytan A (2003) Precipitation of barite by *Myxococcus xanthus*: possible implications for the biogeochemical cycle of barium. *Applied and Environmental Microbiology* **69**, 5722–5.

Granath JW (1989) Structural evolution of the Ardmore Basin, Oklahoma: progressive deformation in the foreland of the Ouachita collision. *Tectonics* **8**, 1015–36.

Hanor JS, (2000) Barite-celestine geochemistry and environments of formation. *Reviews in Mineralogy and Geochemistry* **40**, 193–275.

Infante-Paez L, Cardona L, McCullough B and Slatt R (2017) Seismic analysis of paleotopography and stratigraphic controls on total organic carbon: rich sweet spot distribution in the Woodford Shale, Oklahoma, USA. *Interpretation* **5**, T33–47.

Jackson M and Solheid P (2010) On the quantitative analysis and evaluation of magnetic hysteresis data. *Geochemistry, Geophysics, Geosystems* **11**, Q04Z15. doi: 10.1029/2009GC002932.

Johnson KS (1989) Geologic evolution of the Anadarko Basin. *Oklahoma Geological Survey Circular* **90**, 3–12.

Kastner M (1971) Authigenic feldspars in carbonate rocks. *American Mineralogist* **56**, 403–42.

Kennedy MR, Löhr SC, Fraser LA and Baruch ET (2014) Direct evidence for organic carbon preservation as clay-organic nanocomposites in a Devonian black shale; from deposition to diagenesis. *Earth and Planetary Science Letters* **388**, 59–70.

Kirkland DW, Denison RD, Summers DM and Gormly JR (1992) Geology and organic geochemistry of the Woodford Shale in the Criner Hills and western Arbuckle Mountains, Oklahoma. *Oklahoma Geological Survey Circular* **93**, 38–69.

Kirschvink JL (1980) The least squares line and plane and the analysis of paleomagnetic data. *Geophysics Journal Royal Astronomical Society* **62**, 699–718.

Land LS, Mack LE, Milliken KL and Lynch FK (1997) Burial diagenesis of argillaceous sediment, south Texas Gulf of Mexico sedimentary basin: a reexamination. *Geological Society of America Bulletin* **109**, 2–15.

Landis CR and Castaño JR (1994) Maturation and bulk chemical properties of a suite of solid hydrocarbons. *Organic Geochemistry* **22**, 137–49.

Laughrey CD, Purrazzella PF and Hooghan KN (2017) Petroleum geochemistry and mudstone diagenesis of the Woodford Shale, Anadarko Basin, USA – an integrated approach. In *Unconventional Resources Technology Conference, Austin, Texas, USA, 24–26 July, URTeC-2691776-MS*, 12 pp. doi: 10.15530/urtec-2017-2691776.

Leach DL, Bradley D, Lewchuk MT, Symons DTA, de Marsily G and Brannon J (2001) Mississippi Valley-type lead-zinc deposits through geological time: implications from recent age-dating research. *Mineralium Deposita* **36**, 711–40. doi: 10.1007/s001260100208.

Li Y and Schieber J (2015) On the origin of a phosphate enriched interval in the Chattanooga Shale (Upper Devonian) of Tennessee—a combined sedimentologic, petrographic, and geochemical study. *Sedimentary Geology* **329**, 40–61.

Marsh S and Holland A (2016) Comprehensive fault database and interpretive fault map of Oklahoma. *Oklahoma Geological Survey, Open-File Report OF2-2016*.

Maxbauer DP, Feinberg JM and Fox DL (2016) Magnetic mineral assemblages in soils and paleosols as the basis for paleoprecipitation proxies: a review of magnetic methods and challenges. *Earth-Science Reviews* **155**, 28–48.

McCabe C, Van der Voo R and Ballard MM (1984) Late Paleozoic remagnetization of the Trenton Limestone. *Geophysical Research Letters* **11**, 979–82.

Miceli Romero A and Philp RP (2012) Organic geochemistry of the Woodford Shale, southeastern Oklahoma; how variable can shales be? *American Association of Petroleum Geologists Bulletin* **96**, 493–517.

Migaszewski Z, Starnawska E and Gałuszka A (2007) Gorceixite from the Upper Cambrian rocks of the podwiśniówka mine pit, Holy Cross Mountains (South Central Poland). *Mineralogia* **38**, 171–84.

Milliken KL, Esch WL, Reed RM and Zhang T (2012) Grain assemblages and strong diagenetic overprinting in siliceous mudrocks, Barnett Shale (Mississippian), Fort Worth Basin, Texas, U.S.A. *American Association of Petroleum Geologists Bulletin* **96**, 1553–78.

Milliken K and Olson T (2017) Silica diagenesis, porosity evolution, and mechanical behavior in siliceous mudstones, Mowry Shale (Cretaceous), Rocky Mountains, U.S.A. *Journal of Sedimentary Research* **87**, 366–87.

Mrose ME, Chao ECT, Fahey JJ and Milton C (1961) Norsethite, BaMg$(CO_3)_2$, a new mineral from the Green River Formation, Wyoming. *American Mineralogist* **46**, 420–9.

Nadoll P, Angerer T, Mauk JL, French D and Walsh J (2014) The chemistry of hydrothermal magnetite: a review. *Ore Geology Reviews* **61**, 1–32.

Nelson RA, Lenox LC and Ward BJ (1987) Oriented core: its use, error, and uncertainty. *American Association of Petroleum Geologists Bulletin* **71**, 357–67.

Northcutt RA and Campbell JA (1998) Geologic provinces of Oklahoma. In *Basement Tectonics 12. Proceedings of the International Conferences on Basement Tectonics, vol. 6* (eds JP Hogan and MC Gilbert), pp. 29–37. Dordrecht: Springer. doi: 10.1007/978-94-011-5098-9_2.

Okamoto A, Saishu H, Hirano N and Tsuchiya N (2010) Mineralogical and textural variation of silica minerals in hydrothermal flow-through experiments: implications for quartz vein formation. *Geochimica et Cosmochimica Acta* **74**, 3692–706.

Paterson GA, Zhao Z, Jackson M and Heslop D (2018) Measuring, processing, and analyzing hysteresis data. *Geochemistry, Geophysics, Geosystems* **19**, 1925–45.

Perry Jr. WJ (1989) Tectonic evolution of the Anadarko Basin region, Oklahoma U.S.*United States Geological Survey Bulletin* **1866-A**, 1–19.

https://doi.org/10.1017/S0016756819000360 Published online by Cambridge University Press

Roberts J and Elmore RD (2018) A diagenetic study of the Woodford Shale in the Anadarko Basin, Oklahoma, U.S.A.: evidence for hydrothermal alteration in mineralized fractures. *Interpretation* **6**, 1–13.

Schoenherr J, Littke R, Urai JL, Kukla PA and Rawahi Z (2007) Polyphase thermal evolution in the Infra-Cambrian Ara Group (South Oman Salt Basin) as deduced by maturity of solid reservoir bitumen. *Organic Geochemistry* **38**, 1293–318.

Shand MA (2006) *The Chemistry and Technology of Magnesia*. Hoboken, New Jersey: John Wiley and Sons, Inc., 266 pp.

Shelton KL, Reader JM, Ross LM, Viele GW and Siedeman DW (1986) Ba-rich adularia from the Ouachita Mountains, Arkansas—implications for a post-collisional hydrothermal system. *American Mineralogy* **71**, 916–23.

Steyn JGD and Watson MD (1967) Notes on a new occurrence of norsethite, BaMg $(CO_3)_2$. *The American Mineralogist* **52**, 1770–5.

Tauxe L, Mullender AT and Pick T (1996) Potbellies, wasp-waists, and superparamagnetism in magnetic hysteresis. *Journal of Geophysical Research* **101**, 571–84.

Torsvik TH, Van der Voo R, Preeden U, Niocaill M, Steinberger B, Doubrovine PV, Van Hinsbergen DJ, Domeier M, Gaina C, Tohver E, Meert JG, McCausland PJA, Robin L and Cocks M (2012) Phanerozoic polar wander, palaeogeography and dynamics. *Earth-Science Reviews* **114**, 325–68.

Wang J, Liu J, Peng R, Liu Z, Zhao B, Li Z, Wang Y and Liu C (2014) Gold mineralization in Proterozoic black shales: example from the Haoyaoerhudong gold deposit, northern margin of the North China Craton. *Ore Geology Reviews* **63**, 150–9.

Zhou J, Rush P and Miller R (2015) Barite in the Middle Devonian Marcellus Shale, Appalachian Basin: occurrence, petrography, geochemistry and its implications. In *2015 AAPG Annual Convention and Exhibition, Denver, CO, 31 May – 3 June 2015*. AAPG Datapages/Search and Discovery Article #90216.

https://doi.org/10.1017/S0016756819000360 Published online by Cambridge University Press